Intraindividual Comparison of Gadoxetate Disodium–enhanced MR Imaging and 64-Section Multidetector CT in the Detection of Hepatocellular Carcinoma in Patients with Cirrhosis[1]

Michele Di Martino, MD
Daniele Marin, MD[2]
Antonino Guerrisi, MD
Mahbubeh Baski, MD
Francesca Galati, MD
Massimo Rossi, MD
Stefania Brozzetti, MD
Raffaele Masciangelo, MD
Roberto Passariello, MD
Carlo Catalano, MD

Purpose: To prospectively compare gadoxetate disodium–enhanced magnetic resonance (MR) imaging with multiphasic 64-section multidetector computed tomography (CT) in the detection of hepatocellular carcinoma (HCC) in patients with cirrhosis.

Materials and Methods: Institutional review board approval and informed patient consent were obtained for this prospective study. Fifty-eight patients (39 men, 19 women; mean age, 63 years; age range, 35–84 years) underwent gadoxetate disodium–enhanced MR imaging and multiphasic 64-section multidetector CT. The imaging examinations were performed within 30 days of each other. The two sets of images were qualitatively analyzed in random order by three independent readers in a blinded and retrospective fashion. Using strict diagnostic criteria for HCC, readers classified all detected lesions with use of a four-point confidence scale. The reference standard was a combination of pathologic proof, conclusive imaging findings, and substantial tumor growth at follow-up CT or MR imaging (range of follow-up, 90–370 days). The diagnostic accuracy, sensitivity, and positive predictive value were compared between the two image sets. Interreader variability was assessed. The accuracy of each imaging method was determined by using an adjusted modified χ^2 test.

Results: Eighty-seven HCCs (mean size ± standard deviation, 1.8 cm ± 1.5; range, 0.3–7.0 cm) were confirmed in 42 of the 58 patients. Regardless of lesion size, the average diagnostic accuracy and sensitivity for all readers were significantly greater with gadoxetate disodium–enhanced MR imaging (average diagnostic accuracy: 0.88, 95% confidence interval [CI]: 0.80, 0.97; average sensitivity: 0.85, 95% CI: 0.74, 0.96) than with multidetector CT (average diagnostic accuracy: 0.74, 95% CI: 0.65, 0.82; average sensitivity: 0.69, 95% CI: 0.59, 0.79) ($P < .001$ for each). No significant difference in positive predictive value was observed between the two image sets for each reader. Interreader agreement was good to excellent.

Conclusion: Compared with multiphasic 64-section multidetector CT, gadoxetate disodium–enhanced MR imaging yields significantly higher diagnostic accuracy and sensitivity in the detection of HCC in patients with cirrhosis.

[1] From the Departments of Radiological Sciences (M.D.M., D.M., A.G., M.B., F.G., R.P., C.C.), General Surgery, Division of Organ Transplantation (M.R.), Surgery "P. Valdoni" (S.B.), and Statistics (R.M.), University of Rome Sapienza, Viale Regina Elena 324, Rome 00161, Italy. From the 2008 RSNA Annual Meeting. Received July 22, 2009; revision requested September 10; revision received December 14; accepted January 19, 2010; final version accepted April 12. **Address correspondence to** C.C. (e-mail: *carlo.catalano@uniroma1.it*).
[2] **Current address:** Department of Radiology, Duke University Medical Center; Durham, NC.

Multidetector computed tomography (CT) and magnetic resonance (MR) imaging are the modalities of choice for the diagnosis and follow-up of patients with hepatocellular carcinoma (HCC) and the assessment of tumor burden. Despite improvements in the spatial and temporal resolution of both CT and MR imaging, neither technique is entirely satisfactory for the accurate assessment of HCC in patients with cirrhosis, particularly with regard to smaller lesions (≤2 cm in diameter) (1–4). This problem is partly caused by the lack of characteristic imaging features in a substantial minority of these diminutive lesions and further compounded by the underlying distortion of liver architecture, which may prevent the detection of HCC in these patients.

With the introduction in clinical practice of reticuloendothelial system–specific or hepatobiliary system–specific MR contrast media, MR imaging has the potential to improve the detection and characterization of liver tumors (5). Gadoxetate disodium, which was recently approved by the U.S. Food and Drug Administration, is a paramagnetic, gadolinium-based contrast medium that, after intravenous bolus injection, is partially taken up by functioning hepatocytes and excreted without biotransformation through the biliary system (6). Such a pharmacokinetic profile enables the acquisition in a single examination of a standard dynamic MR study of the liver—which is essential for the comprehensive evaluation of hepatic and vascular disease, particularly in patients with cirrhosis who are at increased risk of developing HCC (7,8). In addition, functional data on the liver and biliary system can be acquired during the delayed hepatobiliary phase. Although preliminary results demonstrated the efficacy of gadoxetate disodium–enhanced MR imaging in the detection and characterization of focal liver lesions during the dynamic and hepatobiliary phases (9–13), to our knowledge only one study has systematically compared gadoxetate disodium–enhanced MR imaging at 3 T with multiphasic contrast medium–enhanced multidetector CT in the detection of HCC in patients with cirrhosis (14).

The purpose of this study was to prospectively compare gadoxetate disodium–enhanced MR imaging with multiphasic 64-section multidetector CT in the detection of HCC in patients with cirrhosis.

Materials and Methods

Gadoxetate disodium was provided free of charge by Bayer Schering Pharma, Berlin, Germany; however, the authors maintained control of the study.

This prospective study was approved by our institutional review board. Although multidetector CT and MR imaging were performed as part of routine medical care, all patients provided written informed consent to use their data for future research.

Study Participants

From February 2007 to October 2008, 250 consecutive patients with cirrhosis were referred to our institution for routine 6-month surveillance or for follow-up diagnostic imaging after curative treatment for HCC. Patients were eligible for enrollment if histologically proved cirrhosis was diagnosed at liver biopsy performed within 2 years before the study, HCC was suspected on the basis of the results of a previous ultrasonographic (US) examination, or α-fetoprotein levels were elevated (>400 ng/mL [400 μg/L]). Patients were excluded if they were younger than 18 years, were pregnant or lactating, had a history of anaphylactoid reaction to iodinated contrast media, had renal failure (serum creatinine level >2.0 mg/dL [177 μmol/L]), had any contraindication to MR imaging (eg, noncompatible biometallic implants or claustrophobia), or had received liver-specific MR contrast media within 2 weeks before the administration of gadoxetate disodium. None of the patients were deemed ineligible for these reasons.

Of the 250 patients who were deemed initially eligible for the study (Fig 1), 192 were excluded for the following reasons: *(a)* the interval between CT and MR imaging was more than 30 days ($n = 140$), *(b)* the patient was lost to follow-up ($n = 26$), *(c)* the patient underwent radiofrequency thermoablation of the tumor during the interval between the two examinations ($n = 9$), *(d)* there was insufficient proof of tumor burden ($n = 8$), *(e)* the patient had subdiagnostic MR images because of an inability to

Advance in Knowledge

- Compared with multiphasic 64-section multidetector CT, gadoxetate disodium–enhanced MR imaging yields significantly higher diagnostic accuracy (0.88 vs 0.74, $P < .001$) and sensitivity (0.85 vs 0.69, $P < .001$) in the detection of hepatocellular carcinoma (HCC) in patients with cirrhosis.

Implication for Patient Care

- Because of the lack of ionizing radiation, MR imaging can provide improved diagnostic performance when compared with 64-section multidetector CT and reduce the risk of cumulative radiation exposure in patients with cirrhosis undergoing serial multidetector CT examinations for the detection of HCC.

Published online
10.1148/radiol.10091334

Radiology 2010; 256:806–816

Abbreviations:
CI = confidence interval
GRE = gradient-recalled echo
HCC = hepatocellular carcinoma
VIBE = volumetric interpolated breath hold

Author contributions:
Guarantors of integrity of entire study, M.D.M., D.M., M.B., F.G., S.B., R.P., C.C.; study concepts/study design or data acquisition or data analysis/interpretation, all authors; manuscript drafting or manuscript revision for important intellectual content, all authors; approval of final version of submitted manuscript, all authors; literature research, M.D.M., D.M., M.B., F.G., M.R., C.C.; clinical studies, M.D.M., D.M., A.G., M.B., F.G., M.R., S.B., R.P., C.C.; statistical analysis, M.D.M., M.B., M.R., R.M., R.P.; and manuscript editing, M.D.M., D.M., A.G., M.B., M.R., R.P., C.C.

Authors stated no financial relationship to disclose.

suspend respiration (n = 6), or *(f)* the patient withdrew consent due to unexpected claustrophobia (n = 3) (15). The remaining 58 patients (mean age, 63 years; age range, 35–84 years) with 109 confirmed liver lesions comprised our study cohort, which included 39 men (mean age, 61 years; age range, 35–81 years) and 19 women (mean age, 65 years; age range, 43–84 years) (Table 1). In 30 patients, multidetector CT was performed before MR imaging (mean interval, 18 days; range, 1–29 days). In the remaining 28 patients, MR imaging preceded multidetector CT (mean interval, 12 days; range, 1–28 days). For all patients, both multidetector CT and MR imaging were performed for clinical patient care.

Multidetector CT Technique

Multiphasic CT was performed by using a 64-section multidetector CT scanner (Somatom Sensation 64; Siemens Medical Systems, Erlangen, Germany) (Table 1). All patients received a nonionic contrast medium (iomeprol, 400 mg of iodine per milliliter [Iomeron 400; Bracco Imaging, Milan, Italy]) at a dose of 1.3 mL (520 mg of iodine) per kilogram of body weight (16). The contrast medium was warmed to 37° and administered with a dual-chamber mechanical power injector (Stellant D CT; Medrad, Indianola, Pa) at a rate of 4–5 mL/sec through an 18-gauge intravenous catheter inserted into an antecubital vein. This was followed by a 40-mL saline flush at the same injection rate.

All patients were positioned head first on the scanning table in the supine position. After acquisition of an anteroposterior digital scout radiograph, patients were scanned craniocaudally from the dome of the liver to the iliac crest before and after intravenous contrast medium administration. Images were obtained during the hepatic arterial, hepatic venous, and delayed phases (25–40, 70, and 180 seconds, respectively, after the start of contrast medium injection). To determine the scanning delay for hepatic arterial phase imaging, the bolus transfer time was assessed by using a bolus-tracking technique with automated scan-triggering software (CARE Bolus CT, Siemens Medical Systems). Arterial phase scanning was started automatically 18 seconds after the trigger threshold (150 HU) was reached at the level of the supraceliac abdominal aorta.

To assess patient radiation dose for a multiphasic, multidetector CT study of the liver, we documented the volumetric CT dose index and dose-length product that were reported by the CT system for each individual scan at the completion of the study (Table 2). The cumulative effective dose for a standard four-phase CT study of the liver was calculated by multiplying the summed dose-length product of all individual scans by a normalized conversion factor for body CT examinations (0.018 $mSv \cdot mGy^{-1} \cdot cm^{-1}$) (17). The cumulative effective dose ranged from 30.5 to 43.1 mSv (mean, 34.6 mSv), depending on the scanning length.

MR Imaging Technique

MR imaging was performed with a 1.5-T unit (Magnetom Avanto, Siemens Medical Systems) with a 36-radiofrequency channel system, which provided a maximum gradient strength of 45 mT/m and a peak slew rate of 200 mT/m/msec. All patients underwent unenhanced,

Figure 1

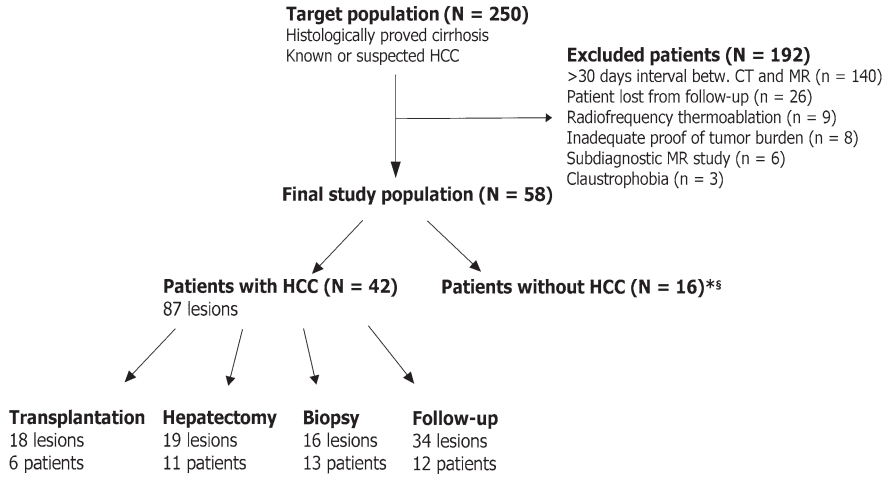

Figure 1: Flowchart of patient enrollment and proof of tumor burden. * = The absence of HCC lesions was confirmed with a combination of clinical and imaging follow-up with either contrast-enhanced CT or MR imaging for a minimum of 6 months. § = Twelve of the 16 patients had no benign or malignant liver lesions. *betw.* = between.

Table 1

Summary of Demographic and Clinical Characteristics of the Study Patients

Parameter	No. of Patients (n = 58)
Race or ethnic group	
White	54 (93)
Black	0 (0)
Hispanic	0 (0)
Asian	1 (2)
Other	3 (5)
Cause of cirrhosis	
Viral hepatitis B	8 (14)
Viral hepatitis C	34 (59)
Alcohol abuse	6 (10)
Nonalcoholic steatohepatitis	4 (7)
Other	6 (10)
Child-Pugh class	
A	30 (52)
B	21 (36)
C	7 (12)
Indication for imaging	
Abnormal findings at US alone	38 (66)
Elevated α-fetoprotein levels (>400 ng/mL) alone	0 (0)
Both of the above	20 (34)

Note.—The mean patient age was 63 years ± 12 (range, 35–84 years). Thirty-nine of the 58 patients (67%) were men and 19 (33%) were women. The mean patient weight was 72 kg ± 12 (range, 48–100 kg). Numbers in parentheses are percentages.

single-breath-hold, T2-weighted two-dimensional turbo spin-echo and T1-weighted two-dimensional dual gradient-recalled echo (GRE) MR imaging (Table 3). After unenhanced imaging, patients received the full dose (0.025 mmol per kilogram of body weight) of gadoxetate disodium (Primovist, Bayer Schering Pharma; 0.1 mL per kilogram of body weight) at a rate of 2 mL/sec through a 20-gauge intravenous catheter placed into a peripheral vein. Contrast medium administration was followed by a 20-mL saline flush at a rate of 2 mL/sec. T1-weighted three-dimensional spoiled GRE volumetric interpolated breath-hold (VIBE) images were obtained 20–40, 60, and 180 seconds after contrast medium injection, during the hepatic arterial, hepatic venous, and delayed phases, respectively, as well as during the liver-specific hepatobiliary phase (20 minutes after contrast medium administration). The optimal imaging delay for the hepatic arterial phase was determined by using a test bolus imaging technique (18).

Qualitative Image Analysis

Three radiologists (C.C., A.G., and D.M., with 18, 10, and 5 years of experience, respectively, in gastrointestinal and hepatobiliary imaging) independently evaluated the multidetector CT and gadoxetate disodium–enhanced MR imaging sets in a retrospective fashion. Images were assessed with a commercially available workstation (Leonardo, Siemens Medical Systems) during two separate reading sessions. To minimize recall bias, each reading session was separated by an interval of 4 weeks. Accordingly, for two readers who were involved with the original interpretation of the imaging studies, a 6-week interval was allowed between the original clinical interpretation and the first reading session. The images of each set were presented in random order to each of the readers at each session by using a computer-generated random-number table. Readers were aware of the imaging phase and knew that all patients had cirrhosis, and thus were at higher risk for developing HCC, but they were unaware of any other clinical information.

Criteria for the diagnosis of HCC were provided to the readers before the first reading session. HCC was unequivocally diagnosed if two criteria (19) were met: *(a)* the lesion was seen to clearly enhance during the hepatic arterial phase and *(b)* the lesion was hypoattenuating or hypointense to the surrounding liver during the hepatic venous and/or delayed phases (washout sign). Because these criteria are highly specific but not very sensitive (20), the following additional imaging findings were regarded as suggestive but not diagnostic of HCC: *(a)* the lesion either had arterial enhancement or was hypoattenuating/hypointense to the surrounding liver during the hepatic venous and/or delayed phases (21–23), *(b)* the lesion had peripheral rim enhancement (fibrous capsule) during the delayed

Table 2

Imaging Parameters, Postprocessing Algorithm, and Radiation Dose for Multiphasic CT of the Liver

CT Parameters	Precontrast Phase	Postcontrast Phases*
Detector configuration	64 (32 × 2) × 0.625 mm	64 (32 × 2) × 0.625 mm
Tube potential (kVp)	120	120
Tube current-time product (mAs)	250	250
Gantry revolution time (sec)	0.33	0.33
Beam pitch	1.0	1.0
Scanning direction	Craniocaudal	Craniocaudal
Scanning time (sec)	4–11	4–11
Reconstructed section thickness (mm)	5.0	3.0
Section overlap (mm)	—	—
Reconstruction kernel	Soft tissue (B20)	Soft tissue (B20)
Volumetric CT dose index (mGy)	10.79	19.15
Dose-length product (mGy · cm)	291–398	468–665

* CT parameters were identical for all postcontrast phases (hepatic arterial, hepatic venous, and delayed phases).

Table 3

MR Imaging Sequences and Parameters

Sequence*	Fat Suppression	TR/TE (msec)†	Flip Angle	Section Thickness (mm)	Matrix Size	Bandwidth (Hz/pixel)	Field of View (cm)	Acquisition Time (sec)
T2-weighted 2D TSE	Not used	4000/76	150°	5–7	192 × 256	260	30–50	36‡
T1-weighted 2D dual GRE	Not used	140/2.2–4.4	90°	5–7	192 × 256	260	30–50	36‡
T1-weighted 3D GRE VIBE§	Used	5.7/2.8	10°	3 (interpolated 2.5)	192 × 256	250	30–50	23

* All sequences were performed with generalized autocalibrating partially parallel acquisition with an acceleration factor of 2. 3D = three-dimensional, TSE = turbo spin-echo, 2D = two-dimensional.

† TE = echo time, TR = repetition time. Parameters are for both opposed-phase and in-phase imaging.

‡ Two breath-hold acquisitions were performed and concatenated for the image reconstruction of the upper abdomen.

§ T1-weighted three-dimensional spoiled GRE VIBE images were acquired 20–40, 60, and 150 seconds after contrast medium administration during the hepatic arterial, hepatic venous, and delayed phases, respectively, and during the liver-specific hepatobiliary phase 20 minutes after the injection.

phase (24), *(c)* the lesion had internal areas suggestive of fatty metamorphosis (defined as areas of low attenuation at unenhanced CT or the demonstration of a substantial decrease in signal intensity at opposed-phase compared with in-phase T1-weighted dual GRE MR imaging) (25), *(d)* the lesion's signal intensity either decreased or increased during the liver-specific hepatobiliary MR imaging phase (17,26,27), and *(e)* the lesion had a mild increase in signal intensity on T2-weighted MR images (3). Although readers were encouraged to follow the above-mentioned criteria for the diagnosis of HCC, the final diagnostic decision was left to the reader's subjective judgment. The readers used well-established imaging criteria for the diagnosis of benign liver lesions (28).

Readers documented the lesion number, size (defined as a lesion's maximum diameter as measured with an electronic ruler on the most representative transverse image), and segmental location according to the anatomic segmentation schemes of Couinaud (29) and Bismuth (30) with use of a standardized template. If a lesion crossed segmental boundaries, it was assigned to the segment with the greatest involvement. Readers also classified all detected lesions as to their likelihood of being HCC by using a four-point confidence scale, as follows: 1, probably absent; 2, indeterminate; 3, probably present; and 4, definitely present. Confidence scores of 3 and 4 represent a positive diagnosis of HCC. HCC lesions were further characterized as hyper- or hypovascular (21).

After identification of all true-positive lesions, all false-negative lesions (lesions assigned a confidence score of 1 or 2 confirmed to be HCC at histopathologic assessment or imaging follow-up) and false-positive lesions (lesions given a score of 3 or 4 in an area of the liver found to be free of lesions at histopathologic assessment or lesions not confirmed to be HCC at imaging follow-up) were retrospectively assessed to identify the causes of diagnostic errors by the same three readers in consensus by using all available preoperative imaging results, histologic findings, and follow-up CT or MR imaging results. In the case of false-negative lesions that could not be seen retrospectively, the three readers searched for common sources of error, including tumor size, technical errors, or the presence of artifacts.

Reference Standard

A composite reference standard was used to diagnose or rule out HCC. The diagnosis of HCC required one of the following conditions: *(a)* pathologic proof of tumor burden obtained after liver transplantation, partial hepatectomy, or biopsy according to the diagnostic criteria established by the terminology for nodular hepatocellular lesions proposed by the International Working Party (31); *(b)* evidence of conclusive criteria for the diagnosis of HCC at imaging (18); or *(c)* demonstration of substantial lesion growth, which was defined as an increase in the longest tumor diameter of more than 5 mm, at follow-up CT and/or MR imaging. The average time between the initial imaging study and surgery was 14 days (range, 3–22 days) for hepatectomy and 75 days (range, 60–90 days) for liver transplantation. In patients who underwent liver transplantation, the explanted livers were cut into 5–10-mm-thick slices by one of three experienced pathologists. The preoperative CT and MR imaging findings were prospectively and directly correlated with the surgical-pathologic findings by an investigator experienced in abdominal imaging (M.D.M.), who was present when the specimen was prepared for evaluation.

On the basis of the above criteria, 87 HCC nodules (mean size, 1.8 cm; range, 0.3–7.0 cm) (Table 4) were diagnosed in 42 of the 58 patients (72%). In five patients with multiple HCC lesions (range, two to four lesions), only one lesion was confirmed at histologic examination; the remaining lesions were confirmed at imaging follow-up of more than 5 months. Nineteen of the 58 patients (33%), including 15 patients who also had HCC, had 22 benign liver lesions (mean size, 1.3 cm; range, 0.6–5.0 cm), including small (≤2 cm) enhancing lesions seen only during the hepatic arterial phase (n = 15), hemangioma (n = 3), and regenerative nodules (n = 4). Four regenerative nodules in three patients were confirmed at histologic examination of the explanted liver. The remaining 18 benign lesions in 16 patients were confirmed at follow-up imaging (mean follow-up, 220 days; range, 180–370 days). In 12 patients, no lesion was identified on the basis of imaging follow-up for a minimum of 12 months.

Statistical Analysis

The diagnostic accuracy, sensitivity, and positive predictive value of multidetector CT and gadoxetate disodium–enhanced MR imaging in the diagnosis of HCC were assessed for all lesions and for the subgroup of lesions 2 cm in diameter or smaller. Lesion size was assessed by a pathologist if the histopathologic section was available; in all other cases, lesion size was measured by one radiologist (M.D.M.) by using the first imaging examination (either CT or MR imaging). Diagnostic accuracy was calculated as the number of lesions confirmed to be HCC at the reference standard (both true-positive and true-negative findings) divided by all test results (ie, true-positive, true-negative, false-positive, and false-negative findings). A modified adjusted χ^2 test was used to test for differences in accuracy, sensitivity, and positive predictive value between MR imaging and multidetector CT, taking into account correlations between multiple lesions within the same patient, correlations between multiple measurements by the three readers (only for accuracy and sensitivity), and correlations between the two procedures in this intraindividual comparison study (32). This χ^2 test was also used to calculate 95% confidence intervals (CIs) for the diagnostic parameters.

Interreader variability among the three readers with regard to lesion detection was assessed by using the unweighted κ statistic. κ values of 0.4 or less were considered indicative of poor agreement, whereas values of 0.41–0.75 and more than 0.75 were considered indicative of good and excellent agreement, respectively (33). Statistical analyses were performed with software (SAS, version 9.1.3; SAS, Cary, NC).

Table 4

Characteristics of HCC Lesions and Proof of Tumor Burden

Parameter	HCC Lesions ($n = 87$)	Benign Lesions ($n = 22$)
Lesion size (cm)		
Mean*	1.8 ± 1.5	1.3 ± 0.9
Range	0.3–7.0	0.6–5.0
No. of lesions per patient		
Mean*	2.1 ± 1.5	1.1 ± 0.3
Range	1–8	1–2
Reference standard†		
Liver transplantation		
No. of lesions	18 (21%)	4 (18%)
No. of patients	6	3
Mean lesion size (cm)*	1.6 ± 1.4	0.76 ± 0.5
Interval between MR imaging and CT (d)*	72 ± 17	82 ± 0.5
Partial hepatectomy		
No. of lesions	19 (22%)	0 (0%)
No. of patients‡	11	0
Mean lesion size (cm)*	3.1 ± 1.5	...
Interval between MR imaging and CT (d)*	14 ± 7	...
Percutaneous liver biopsy		
No. of lesions	16 (18%)	0 (0%)
No. of patients‡	13	0
Mean lesion size (cm)*	2.1 ± 1.0	...
Interval between MR imaging and CT (d)*		...
Imaging follow-up		..
No. of lesions	34 (39%)	18 (82%)
No. of patients	12	16
Mean lesion size (cm)*	2.1 ± 1.3	1.4 ± 0.9
Mean follow-up (d)§	109 (90–180)	220 (180–370)

Note.—The average time between the initial imaging study and surgery was 14 days (range, 3–22 days) for hepatectomy and 75 days (range, 60–90 days) for liver transplantation.

* Data are means ± standard deviations.

† There were no characteristic imaging findings.

‡ In five patients with multiple HCC lesions (range, two to four lesions), only one lesion was confirmed at histologic examination; the remaining lesions were confirmed at imaging follow-up of more than 5 months.

§ Numbers in parentheses are the range.

Results

Diagnostic Accuracy

For all HCC lesions and for lesions 2 cm or smaller, the diagnostic accuracy across the three readers was significantly greater with gadoxetate disodium–enhanced MR imaging than with multidetector CT (0.88 [95% CI: 0.80, 0.97] vs 0.74 [95% CI: 0.65, 0.82], respectively, for all lesions and 0.84 [95% CI: 0.73, 0.95] vs 0.67 [95% CI: 0.56, 0.79] for lesions ≤2 cm; $P < .001$) (Table 5).

Sensitivity and False-Negative Findings

For all HCC lesions and for lesions 2 cm or smaller, the sensitivity across the three readers was significantly greater with gadoxetate disodium–enhanced MR imaging than with multidetector CT (0.85 [95% CI: 0.74, 0.96] vs 0.69 [95% CI: 0.59, 0.79], respectively, for all lesions, $P < .001$; 0.77 [95% CI: 0.61, 0.93] vs 0.56 [95% CI: 0.42, 0.71] for lesions ≤2 cm, $P = .003$) (Table 6).

Of the 87 confirmed HCC lesions in 42 patients—including 79 hypervascular and eight hypovascular tumor nodules—49 lesions (56%) in 35 patients were detected by all readers on both image sets (Fig 2). Thirty-eight lesions, most of which were 2 cm or smaller ($n = 34$), were missed or assigned a low confidence score (score of 1 or 2) by at least one reader on at least one image set. Fourteen HCC nodules (mean size, 1.2 cm; range, 0.3–2.2 cm) in eight patients that could not be detected

Table 5

Diagnostic Accuracy in the Detection of HCC

Lesion Group and Imaging Modality	Reader 1	Reader 2	Reader 3	Average across Readers
All lesions ($n = 109$)				
Multiphasic 64-section CT	0.72 (0.62, 0.82)	0.74 (0.65, 0.82)	0.76 (0.66, 0.86)	0.74 (0.65, 0.82)
Gadoxetic acid–enhanced MR imaging	0.87 (0.77, 0.96)	0.92 (0.84, 0.99)	0.87 (0.76, 0.97)	0.88 (0.80, 0.97)
Difference between MR imaging and CT	0.15 (0.05, 0.24)	0.18 (0.10, 0.27)	0.11 (0.03, 0.18)	0.15 (0.08, 0.22)
P value	.0072	.0010	.0100	.0001
Lesions ≤2 cm ($n = 75$)				
Multiphasic 64-section CT	0.66 (0.53, 0.78)	0.66 (0.54, 0.77)	0.71 (0.58, 0.85)	0.67 (0.56, 0.79)
Gadoxetic acid–enhanced MR imaging	0.83 (0.53, 0.78)	0.89 (0.79, 0.98)	0.82 (0.68, 0.96)	0.84 (0.73, 0.95)
Difference between MR imaging and CT	0.17 (0.05, 0.29)	0.23 (0.11, 0.35)	0.10 (0.01, 0.20)	0.17 (0.08, 0.26)
P value	.0099	.0018	.0415	.0003

Note.—Numbers in parentheses are the 95% CIs.

Table 6

Sensitivity for the Detection of HCC

Lesion Group and Imaging Modality	Reader 1	Reader 2	Reader 3	Average across Readers
All lesions ($n = 109$)				
Multiphasic 64-section CT	0.66 (0.53, 0.78) [57/87]	0.70 (0.60, 0.80) [61/87]	0.71 (0.59, 0.83) [62/87]	0.69 (0.59, 0.79)
Gadoxetic acid–enhanced MR imaging	0.82 (0.69, 0.94) [71/87]	0.91 (0.81, 1.00) [79/87]	0.83 (0.69, 0.97) [72/87]	0.85 (0.74, 0.96)
Difference between MR imaging and CT	0.16 (0.03, 0.29)	0.21 (0.11, 0.30)	0.11 (0.02, 0.21)	0.16 (0.07, 0.25)
P value	.0289	.0017	.0274	.0004
Lesions ≤2 cm ($n = 75$)				
Multiphasic 64-section CT	0.53 (0.36, 0.70) [29/55]	0.56 (0.41, 0.72) [31/55]	0.60 (0.43, 0.77) [33/55]	0.56 (0.42, 0.71)
Gadoxetic acid–enhanced MR imaging	0.73 (0.55, 0.91) [40/55]	0.85 (0.71, 1.00) [47/55]	0.73 (0.53, 0.92) [40/55]	0.77 (0.61, 0.93)
Difference between MR imaging and CT	0.20 (0.02, 0.38)	0.29 (0.13, 0.45)	0.13 (−0.00, 0.26)	0.21 (0.07, 0.34)
P value	.0457	.0031	.0771	.0031

Note.—Numbers in parentheses are the 95% CIs. Numbers in brackets are numbers of lesions.

Figure 2

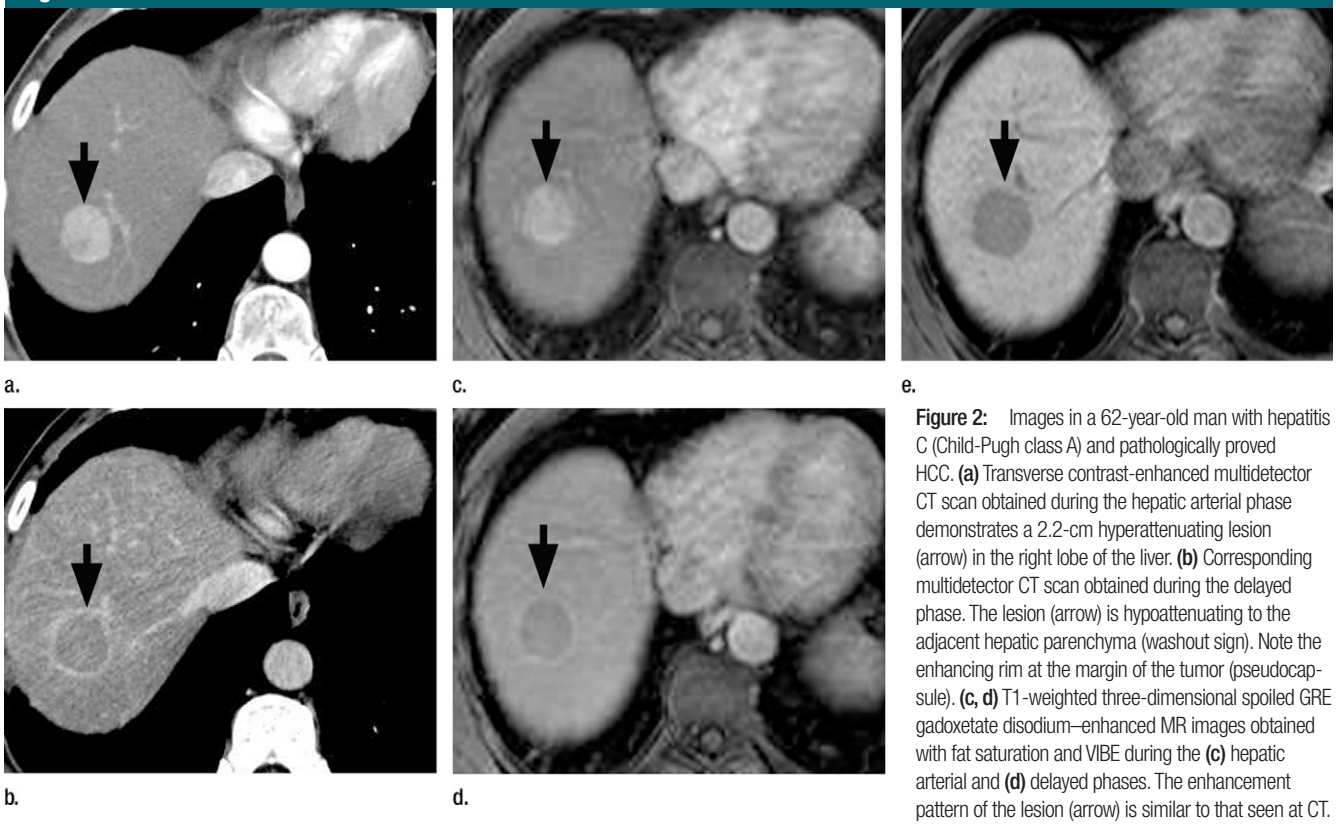

Figure 2: Images in a 62-year-old man with hepatitis C (Child-Pugh class A) and pathologically proved HCC. **(a)** Transverse contrast-enhanced multidetector CT scan obtained during the hepatic arterial phase demonstrates a 2.2-cm hyperattenuating lesion (arrow) in the right lobe of the liver. **(b)** Corresponding multidetector CT scan obtained during the delayed phase. The lesion (arrow) is hypoattenuating to the adjacent hepatic parenchyma (washout sign). Note the enhancing rim at the margin of the tumor (pseudocapsule). **(c, d)** T1-weighted three-dimensional spoiled GRE gadoxetate disodium–enhanced MR images obtained with fat saturation and VIBE during the **(c)** hepatic arterial and **(d)** delayed phases. The enhancement pattern of the lesion (arrow) is similar to that seen at CT. **(e)** Corresponding MR image obtained during the liver-specific hepatobiliary phase, 20 minutes after contrast medium administration. The lesion (arrow) is markedly hypointense to the highly enhanced background liver, a finding consistent with malignancy.

at multidetector CT were correctly identified with gadoxetate disodium–enhanced MR imaging (Fig 3). One small HCC (0.8 cm) in a patient with more than three HCC lesions was missed with gadoxetate disodium–enhanced MR imaging but detected with multidetector CT. Five HCC lesions in two patients were identified at gadoxetate disodium–enhanced MR imaging during the hepatobiliary phase but could not be detected during the dynamic vascular phase at either MR imaging or multidetector CT.

On gadoxetate disodium–enhanced MR images obtained during the hepatobiliary phase, most HCC lesions (80 of 87 lesions, 92%) were hypointense to the surrounding liver parenchyma; only a few lesions were isointense (five of 87, 6%) or hyperintense (two of 87, 2%) (Fig 4).

Figure 3

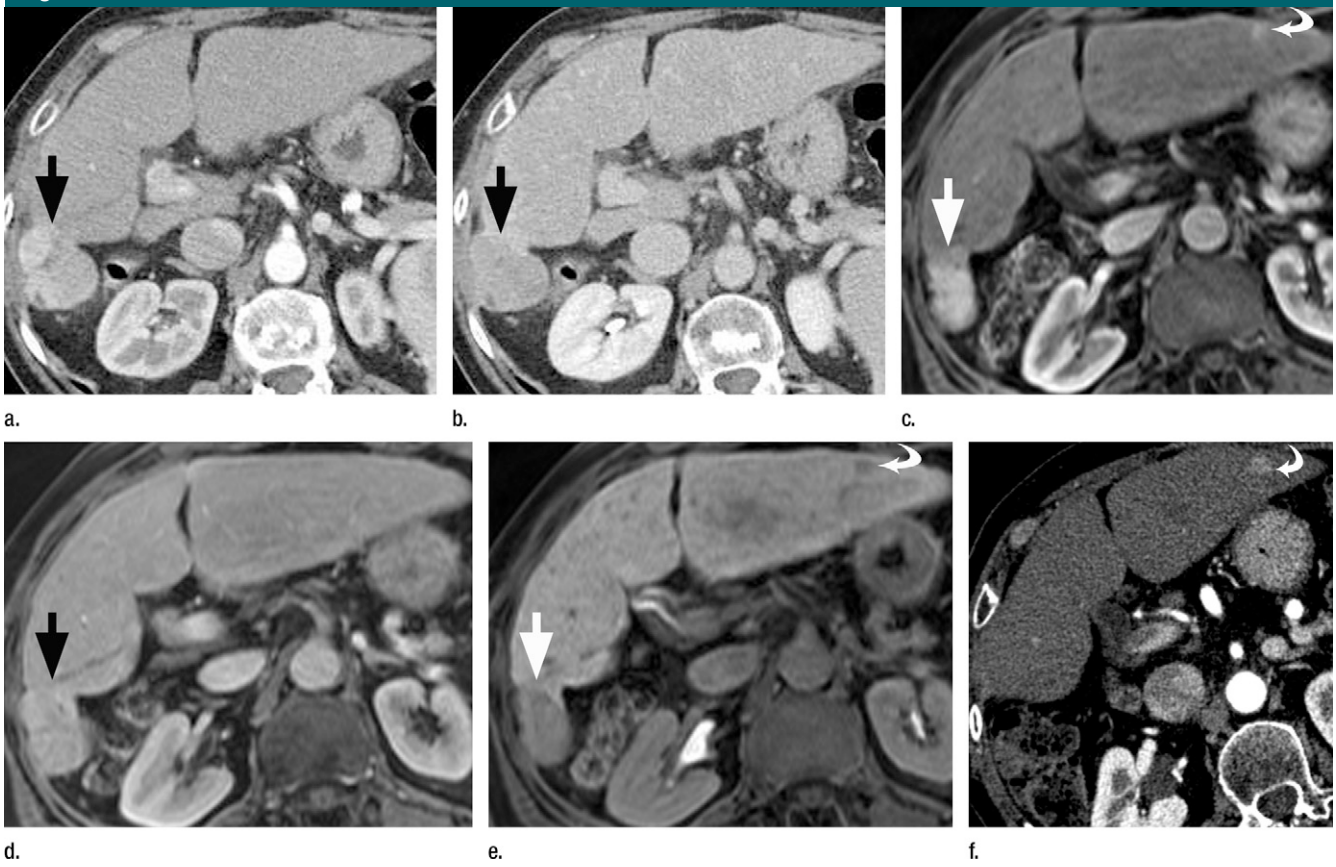

Figure 3: Images in a 73-year-old woman with cryptogenic cirrhosis (Child-Pugh class A) and two HCCs. **(a)** Transverse contrast-enhanced multidetector CT scan obtained during the hepatic arterial phase demonstrates a 4-cm, subcapsular, hyperattenuating lesion (arrow) in the right lobe of the liver. **(b)** Corresponding multidetector CT scan obtained during the delayed phase shows that the lesion (arrow) is hypoattenuating to the adjacent hepatic parenchyma (washout sign). **(c, d)** T1-weighted three-dimensional spoiled GRE gadoxetate disodium–enhanced MR images obtained with fat saturation and VIBE during the **(c)** hepatic arterial and **(d)** delayed phases. The enhancement pattern of the lesion (straight arrow) is similar to that seen at multidetector CT. A second high-signal-intensity lesion (curved arrow in **c**) measuring 1 cm was identified only during the hepatic arterial phase. **(e)** Corresponding MR image obtained during the liver-specific hepatobiliary phase, 20 minutes after contrast medium administration. Both lesions (arrows) are markedly hypointense to the highly enhanced background liver, a finding consistent with malignancy. **(f)** Multidetector CT scan obtained at 6-month follow-up shows resection of the larger lesion and a substantial interval increase (>30%) in the size of the smaller lesion (curved arrow). Biopsy of the smaller lesion was diagnostic of HCC.

Positive Predictive Value and False-Positive Findings

No significant difference was observed in the average positive predictive value between the two image sets (Table 7). At retrospective analysis, there were three false-positive findings with gadoxetate disodium–enhanced MR imaging (mean lesion size, 1.3 cm; range, 1.0–1.5 cm), including two enhancing lesions seen only during the hepatic arterial phase for one reader and one regenerative nodule for another. The regenerative nodule was not seen at multidetector CT. There were 14 false-positive findings with multidetector CT (mean lesion size, 1.1 cm; range, 0.6–2.2 cm), including six enhancing lesions seen only during the hepatic arterial phase for two readers and one enhancing lesion seen only during the hepatic arterial phase and one capillary hemangioma for one reader. Twelve of the 14 false-positive findings at multidetector CT were correctly interpreted with gadoxetate disodium–enhanced MR imaging.

Interreader Agreement

For each image set, there was good to excellent (κ = 0.70–0.86) reader agreement for the detection of HCC lesions among the three readers.

Discussion

The results of our study demonstrate that, compared with multiphasic 64-section multidetector CT, gadoxetate disodium–enhanced MR imaging yields significantly higher diagnostic accuracy and sensitivity for the detection of HCC in patients with cirrhosis ($P < .001$ for both comparisons). Our results, which showed good to excellent agreement among the three readers, were

Figure 4

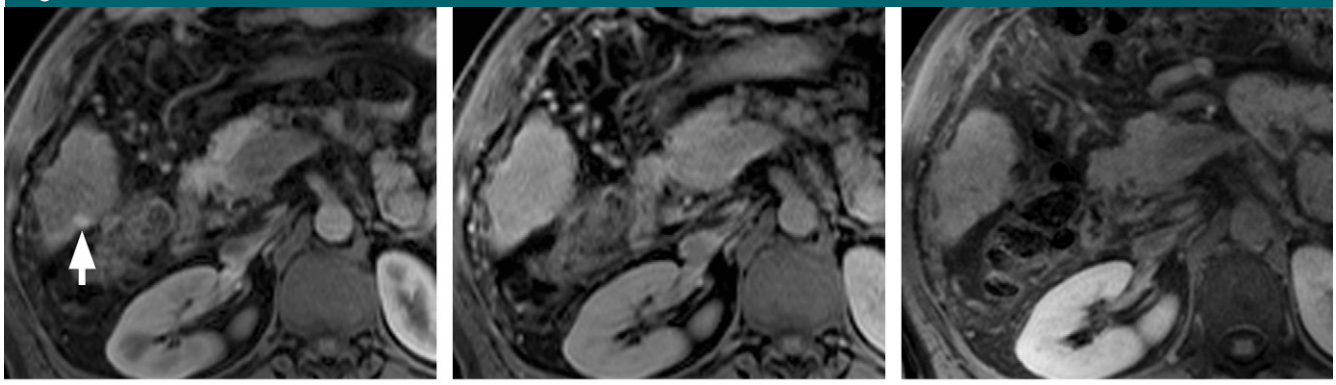

a. b. c.

Figure 4: Images in a 45-year-old man with hepatitis C (Child-Pugh class B) and two HCCs (confirmed at transplantation). **(a)** Transverse T1-weighted three-dimensional spoiled GRE gadoxetate disodium–enhanced MR image obtained with fat saturation and VIBE during the hepatic arterial phase demonstrates a 0.5-cm subcapsular lesion (arrow) with high signal intensity in the right lobe of the liver. **(b, c)** Corresponding MR images obtained during the **(b)** delayed and **(c)** liver-specific hepatobiliary phases. The lesion is isointense to adjacent hepatic parenchyma. Because of the small lesion size, the subcapsular location, and the lack of the washout sign, this lesion was assigned a low score for malignancy (score of 1) by all readers; however, it was confirmed to be HCC at pathologic analysis of the explanted liver.

Table 7

Positive Predictive Value for the Detection of HCC

Lesion Group and Imaging Modality	Reader 1	Reader 2	Reader 3	Average across Readers
All lesions ($n = 109$)				
Multiphasic 64-section CT	0.93 (0.84, 0.98) [57/61]	0.91 (0.84, 0.98) [61/67]	0.94 (0.80, 0.96) [62/66]	0.92 (0.82, 0.97)
Gadoxetic acid–enhanced MR imaging	1.00 (0.95, 1.00) [71/71]	0.98 (0.91, 0.99) [79/81]	0.99 (0.93, 0.99) [72/73]	0.98 (0.93, 0.99)
Difference between MR imaging and CT*	0.07 (−0.35, 0.16)	0.06 (−0.018, 0.016)	0.053 (−0.023, 0.14)	0.062 (0.02, 0.11)
Lesions ≤2 cm ($n = 75$)				
Multiphasic 64-section CT	0.88 (0.72, 0.96) [30/34]	0.84 (0.68, 0.94) [31/37]	0.92 (0.77, 0.98) [33/36]	0.88 (0.72, 0.96)
Gadoxetic acid–enhanced MR imaging	1.00 (0.91, 0.99) [40/40]	0.96 (0.86, 0.99) [47/49]	0.97 (0.83, 0.99) [40/41]	0.98 (0.86, 0.99)
Difference between MR imaging and CT*	0.12 (0.01, 0.23)	0.12 (−0.01, 0.25)	0.052 (−0.04, 0.16)	0.098 (−0.042, 0.25)

Note.—Numbers in parentheses are 95% CIs. Numbers in brackets are numbers of lesions.

* No significant difference was observed between multidetector CT and gadoxetic acid–enhanced MR imaging for all lesions and lesions 2 cm or smaller.

confirmed for all HCC lesions and for lesions 2 cm in diameter or smaller (diagnostic accuracy, $P < .001$; sensitivity, $P = .003$). In particular, our data showed that 14 tumor foci (mean size, 1.2 cm) in eight patients were detected only with gadoxetate disodium–enhanced MR imaging.

Our data corroborate the results of a recent study by Kim et al (14), which showed a trend, although not statistically significant, toward improved diagnostic accuracy with gadoxetate disodium–enhanced MR imaging compared with multidetector CT for the detection of HCC in patients with cirrhosis, particularly for smaller lesions (≤2 cm). This finding has important clinical implications. The superior tumor detection with gadoxetate disodium–enhanced MR imaging could enable the diagnosis of small HCCs in patients with cirrhosis and a positive screening test. This offers the possibility of clinical interventions when liver function is still preserved, and potential curative therapies can be performed, including transplantation, hepatic resection, and percutaneous tumor ablation techniques (34–36).

In accordance with the study by Kim et al (14), we found that gadoxetate disodium–enhanced MR imaging yielded fewer false-positive findings compared with multiphasic 64-section multidetector CT, although there was no statistically significant difference in positive predictive value. The frequency of false-positive findings—which can be related to a variety of causes, including dysplastic nodules, areas of confluent hepatic fibrosis, nontumorous arterioportal shunts, and hemangiomas (37)—has increased substantially with recent advances in cross-sectional imaging techniques. Such findings present two problems: They expose patients with cirrhosis to the risk of unnecessarily high recall or biopsy rates, which could lead to increased patient anxiety and cost, and, for patients on the liver transplantation waiting list, they can erroneously increase their assignment priority. Larger studies must be performed to determine more adequately

the effectiveness of gadoxetate disodium–enhanced MR imaging for improving the specificity for the diagnosis of HCC in patients with cirrhosis.

Along with improved capabilities in the detection of HCC, an additional benefit of MR imaging compared with multidetector CT is the absence of radiation hazards. This attribute is particularly important owing to the increasingly higher radiation burden from medical exposures (38) and concern about the increased risk of lifetime cancer incidence associated with CT (39). By applying a normalized conversion factor of 0.018 mSv · mGy^{-1} · cm (19) in our study, we estimated a cumulative effective dose of 30.5–43.1 mSv for a four-phase multidetector CT examination of the liver. That dose is remarkably higher than the average effective dose for a conventional single-phase CT examination of the abdomen and pelvis (8 mSv) (40), which has been associated with an estimated lifetime attributable risk of death from cancer of 0.02% (39). Although the effective dose is an imprecise metric and the radiation risk is usually justified by the diagnostic information obtained with a CT study, this risk must be considered, particularly in patients with cirrhosis who are exposed to serial examinations with use of multiple-acquisition protocols.

In our study, a substantial minority of patients (nine of 84, 11%) were excluded from the final analysis because of subdiagnostic MR images owing to the patient's inability to suspend respiration or the patient's withdrawal of consent due to unexpected claustrophobia. Although we have no explanation for this observation, we postulate that it may be related to lower patient compliance with the longer examination time of MR imaging compared with that of multidetector CT. With the proliferation of 3-T whole-body MR systems, along with new time-efficient parallel imaging techniques, the number of noncompliant patients is likely to decrease owing to faster data sampling and shorter acquisition times (41).

Some potential limitations of our study merit consideration. First, multidetector CT and MR imaging were restricted to patients who had an abnormal screening test. Although this approach is in accordance with the recent evidence-based guidelines of the American Association for the Study of Liver Diseases (19), it could have resulted in selection bias and prevented us from comparing our data with those reported in large surveillance populations of patients with cirrhosis (1–4). Second, pathologic confirmation of HCC was obtained in only 53 of the 87 nodules (61%). However, the presence of other proved HCC tumors, the small size of many nodules, and the patient's clinical history frequently made biopsy of individual lesions unnecessary or impractical from an ethical standpoint. Furthermore, for all patients whose liver lesions were not verified at histopathologic examination, a substantial increase in lesion size (>5 mm) was confirmed at follow-up with multidetector CT or MR imaging. Third, because pathologic proof was not obtained for all lesions, we could not evaluate the effect of tumor grade on lesion signal intensity during the liver-specific hepatobiliary phase. Fourth, because two of the three readers were also involved in the prospective assessment of CT and MR images, recall bias cannot be excluded. Fifth, the follow-up interval for some benign lesions was relatively short—as little as 6 months. Finally, as per the manufacturer's labeling instructions, gadoxetate disodium–enhanced hepatobiliary phase imaging was performed 20 minutes after contrast medium administration. Although this interval has been shown to yield the highest conspicuity for liver tumors in patients with normal liver function (9), recent evidence indicates that contrast medium uptake and biliary excretion may be delayed in patients with cirrhosis (10). Future studies are warranted to determine the interval that maximizes the conspicuity of HCC at gadoxetate disodium–enhanced MR imaging during the hepatobiliary phase in patients with cirrhosis.

In summary, compared with multiphasic 64-section multidetector CT, gadoxetate disodium–enhanced MR imaging yields significantly higher diagnostic accuracy and sensitivity in the detection of HCC in patients with cirrhosis.

Acknowledgments: We express our gratitude to Richard S. Youngblood, MA, MFA, for his invaluable help in manuscript revision and to Carsten Schwenke, PhD, for his assistance with the statistical analysis.

References

1. Peterson MS, Baron RL, Marsh JW Jr, Oliver JH 3rd, Confer SR, Hunt LE. Pretransplantation surveillance for possible hepatocellular carcinoma in patients with cirrhosis: epidemiology and CT-based tumor detection rate in 430 cases with surgical pathologic correlation. Radiology 2000;217(3):743–749.
2. Lim JH, Kim CK, Lee WJ, et al. Detection of hepatocellular carcinomas and dysplastic nodules in cirrhotic livers: accuracy of helical CT in transplant patients. AJR Am J Roentgenol 2000;175(3):693–698.
3. Krinsky GA, Lee VS, Theise ND, et al. Hepatocellular carcinoma and dysplastic nodules in patients with cirrhosis: prospective diagnosis with MR imaging and explantation correlation. Radiology 2001;219(2):445–454.
4. Krinsky GA, Lee VS, Theise ND, et al. Transplantation for hepatocellular carcinoma and cirrhosis: sensitivity of magnetic resonance imaging. Liver Transpl 2002;8(12):1156–1164.
5. Semelka RC, Helmberger TK. Contrast agents for MR imaging of the liver. Radiology 2001;218(1):27–38.
6. Gadoxetate disodium: label and approval history. U.S. Food and Drug Administration Web site. http://www.accessdata.fda.gov/scripts/cder/drugsatfda/index.cfm?fuseaction=Search.Label_ApprovalHistory#apphist. Updated September 6, 2010. Accessed September 6, 2010.
7. Yamashita Y, Mitsuzaki K, Yi T, et al. Small hepatocellular carcinoma in patients with chronic liver damage: prospective comparison of detection with dynamic MR imaging and helical CT of the whole liver. Radiology 1996;200(1):79–84.
8. Oi H, Murakami T, Kim T, Matsushita M, Kishimoto H, Nakamura H. Dynamic MR imaging and early-phase helical CT for detecting small intrahepatic metastases of hepatocellular carcinoma. AJR Am J Roentgenol 1996;166(2):369–374.
9. Vogl TJ, Kümmel S, Hammerstingl R, et al. Liver tumors: comparison of MR imaging with Gd-EOB-DTPA and Gd-DTPA. Radiology 1996;200(1):59–67.
10. Hammerstingl R, Huppertz A, Breuer J, et al. Diagnostic efficacy of gadoxetic acid (Primovist) enhanced MRI and spiral CT for a therapeutic strategy: comparison with intraoperative and histopathologic findings in focal liver lesions. Eur Radiol 2008;18(3):457–467.

11. Bluemke DA, Sahani D, Amendola M, et al. Efficacy and safety of MR imaging with liver-specific contrast agent: U.S. multicenter phase III study. Radiology 2005;237(1):89–98.

12. Huppertz A, Balzer T, Blakeborough A, et al. Improved detection of focal liver lesions at MR imaging: multicenter comparison of gadoxetic acid–enhanced MR images with intraoperative findings. Radiology 2004;230(1):266–275.

13. Halavaara J, Breuer J, Ayuso C, et al. Liver tumor characterization: comparison between liver-specific gadoxetic acid disodium–enhanced MRI and biphasic CT—a multicenter trial. J Comput Assist Tomogr 2006;30(3):345–354.

14. Kim SH, Kim SH, Lee J, et al. Gadoxetic acid–enhanced MRI versus triple-phase MDCT for the preoperative detection of hepatocellular carcinoma. AJR Am J Roentgenol 2009;192(6):1675–1681.

15. Bossuyt PM, Reitsma JB, Bruns DE, et al. Towards complete and accurate reporting of studies of diagnostic accuracy: the STARD initiative. Radiology 2003;226(1):24–28.

16. Heiken JP, Brink JA, McClennan BL, Sagel SS, Crowe TM, Gaines MV. Dynamic incremental CT: effect of volume and concentration of contrast material and patient weight on hepatic enhancement. Radiology 1995;195(2):353–357.

17. Huda W, Ogden KM, Khorasani MR. Converting dose-length product to effective dose at CT. Radiology 2008;248(3):995–1003.

18. Kanematsu M, Semelka RC, Matsuo M, et al. Gadolinium-enhanced MR imaging of the liver: optimizing imaging delay for hepatic arterial and portal venous phases—a prospective randomized study in patients with chronic liver damage. Radiology 2002;225(2):407–415.

19. Bruix J, Sherman M; Practice Guidelines Committee, American Association for the Study of Liver Diseases. Management of hepatocellular carcinoma. Hepatology 2005;42(5):1208–1236.

20. Forner A, Vilana R, Ayuso C, et al. Diagnosis of hepatic nodules 20 mm or smaller in cirrhosis: prospective validation of the noninvasive diagnostic criteria for hepatocellular carcinoma. Hepatology 2008;47(1):97–104.

21. Bolondi L, Gaiani S, Celli N, et al. Characterization of small nodules in cirrhosis by assessment of vascularity: the problem of hypovascular hepatocellular carcinoma. Hepatology 2005;42(1):27–34.

22. Yu JS, Chung JJ, Kim JH, Kim KW. Large (>or=2 cm) non-hypervascular nodules depicted on MRI in the cirrhotic liver: fate and implications. Clin Radiol 2008;63(10):1121–1130.

23. Chung JJ, Yu JS, Kim JH, Kim MJ, Kim KW. Nonhypervascular hypoattenuating nodules depicted on either portal or equilibrium phase multiphasic CT images in the cirrhotic liver. AJR Am J Roentgenol 2008;191(1):207–214.

24. Grazioli L, Olivetti L, Fugazzola C, et al. The pseudocapsule in hepatocellular carcinoma: correlation between dynamic MR imaging and pathology. Eur Radiol 1999;9(1):62–67.

25. Martín J, Sentís M, Zidan A, et al. Fatty metamorphosis of hepatocellular carcinoma: detection with chemical shift gradient-echo MR imaging. Radiology 1995;195(1):125–130.

26. Huppertz A, Haraida S, Kraus A, et al. Enhancement of focal liver lesions at gadoxetic acid–enhanced MR imaging: correlation with histopathologic findings and spiral CT—initial observations. Radiology 2005;234(2):468–478.

27. Frericks BB, Loddenkemper C, Huppertz A, et al. Qualitative and quantitative evaluation of hepatocellular carcinoma and cirrhotic liver enhancement using Gd-EOB-DTPA. AJR Am J Roentgenol 2009;193(4):1053–1060.

28. Elsayes KM, Narra VR, Yin Y, Mukundan G, Lammle M, Brown JJ. Focal hepatic lesions: diagnostic value of enhancement pattern approach with contrast-enhanced 3D gradient-echo MR imaging. RadioGraphics 2005;25(5):1299–1320.

29. Couinaud C. Le foie: études anatomiques et chirurgicales. Paris, France: Masson, 1957;9–12.

30. Bismuth H. Surgical anatomy and anatomical surgery of the liver. World J Surg 1982;6(1):3–9.

31. Terminology of nodular hepatocellular lesions. International Working Party. Hepatology 1995;22(3):983–993.

32. Schwenke C, Busse R. Analysis of differences in proportions from clustered data with multiple measurements in diagnostic studies. Methods Inf Med 2007;46(5):548–552.

33. Landis JR, Koch GG. The measurement of observer agreement for categorical data. Biometrics 1977;33(1):159–174.

34. Bigourdan JM, Jaeck D, Meyer N, et al. Small hepatocellular carcinoma in Child A cirrhotic patients: hepatic resection versus transplantation. Liver Transpl 2003;9(5):513–520.

35. Figueras J, Jaurrieta E, Valls C, et al. Resection or transplantation for hepatocellular carcinoma in cirrhotic patients: outcomes based on indicated treatment strategy. J Am Coll Surg 2000;190(5):580–587.

36. Livraghi T, Meloni F, Di Stasi M, et al. Sustained complete response and complications rates after radiofrequency ablation of very early hepatocellular carcinoma in cirrhosis: is resection still the treatment of choice? Hepatology 2008;47(1):82–89.

37. Brancatelli G, Baron RL, Peterson MS, Marsh W. Helical CT screening for hepatocellular carcinoma in patients with cirrhosis: frequency and causes of false-positive interpretation. AJR Am J Roentgenol 2003;180(4):1007–1014.

38. Mettler FA Jr, Thomadsen BR, Bhargavan M, et al. Medical radiation exposure in the U.S. in 2006: preliminary results. Health Phys 2008;95(5):502–507.

39. Brenner DJ, Hall EJ. Computed tomography: an increasing source of radiation exposure. N Engl J Med 2007;357(22):2277–2284.

40. Mettler FA Jr, Huda W, Yoshizumi TT, Mahesh M. Effective doses in radiology and diagnostic nuclear medicine: a catalog. Radiology 2008;248(1):254–263.

41. Chang KJ, Kamel IR, Macura KJ, Bluemke DA. 3.0-T MR imaging of the abdomen: comparison with 1.5 T. RadioGraphics 2008;28(7):1983–1998.